LRP 603/98 mars 1998

TOPOLOGIC STUDY OF A MAGNETIC PERTURBATION IN A 3-D FREE BOUNDARY PLASMA EQUILIBRIUM

O. Fischer, W.A. Cooper

Accepted for publication in
Plasma Phys. & Contr. Fusion

Topologic Study of a Magnetic Perturbation in a 3-D Free Boundary Plasma Equilibrium

O. Fischer* and W.A. Cooper
Centre de Recherches en Physique des Plasmas, Association Euratom-Confédération Suisse, Ecole Polytechnique Fédérale de Lausanne, CRPP-PPB,CH-1015 Lausanne, Switzerland

March 30, 1998

*E-mail: Olivier.Fischer@crpp.uhd.epfl.ch

Abstract

We have investigated the topological modification of an equilibrium with nested magnetic flux surfaces computed with the free boundary VMEC code subject to an applied magnetic field perturbation. Magnetic field lines are traced in the domain interior to the plasma-vacuum interface either in the coordinates of the VMEC code (s, u, v) or using canonical coordinates (Ψ, θ^*, v) that allow a Hamiltonian description of the magnetic field lines. The perturbation models the effect of the magnetic flux leakage from the saturated iron core of the JET device. Island formation around resonant surfaces near the boundary is observed, but these islands do not overlap.The Chirikov parameters and the Liapunov exponents that are specifically calculated verify this.

1 Introduction

We have studied the topological modification of a three dimensional (3-D) free boundary equilibrium plasma subject to a magnetic field perturbation. A 3-D magnetohydrodynamic (MHD) tokamak equilibrium with finite ripple due to the discrete toroidal coils is calculated with the free boundary VMEC code [1, 2, 3]. The magnetic perturbation is computed using the Biot-Savart Law applied to the superposition of sets of current carrying filaments of slightly different shapes that yield a toroidally modulated vertical field. To visualize the topological modification, we have to trace the magnetic field lines inside the plasma boundary. There are several possible approaches to treat the problem. The first one consists to solve the equations of magnetic field lines in the VMEC coordinates using directly the magnetic field components in the contravariant representation B^s, B^u and B^v. This method does not impose any approximations concerning the magnetic fields. But in physics, we often study Hamiltonian systems. The incompressibility of the magnetic field $\mathbf{B}$ allows a Hamiltonian representation for the magnetic field lines. The main problem consists to identify the canonical coordinates and the Hamiltonian function of the system. We have two possibilities. The first one consists in taking an analytic Hamiltonian and thus some approximations are made. The canonical coordinates in this case correspond to the magnetic coordinates (ψ, θ^*, v). On the other hand, if we do not want to make any approximations, we have to compute the Hamiltonian in the canonical coordinates (Ψ, θ^*, v) numerically.

To realize these different methods, we have developed the **M**agnetic **F**ield **L**ine **T**racing **3-D**imension (**MFLT3D**) code. This code allows to trace the magnetic field lines inside the plasma boundary with the help of magnetic fields (first version), with an analytic Hamiltonian (second version) and finally with a numerical Hamiltonian (third version). All these versions need the output of the 3-D free boundary VMEC code.

We are interested to determine the differences or the common points between these three methods for a given system (equilibrium + magnetic perturbation). Therefore, we have studied the influence of the magnetic flux leakage from the saturated iron core of a JET Tokamak equilibrium. This example allows us to demonstrate that the calculation of the numerical Hamiltonian is possible and that the differences with the magnetic field lines traced directly from the magnetic fields are not large.

Concerning the organization of the paper, in the first section we present a brief review of the theory: the VMEC coordinates, the magnetic coordinates with the analytic Hamiltonian and the calculation of canonical coordinates.

In the second section, we will examine the main differences between the three methods that we have outlined above.

2 Review of the theory

2.1 The 3-D free boundary VMEC equilibrium code

We use the 3-D free boundary VMEC equilibrium code [1, 2, 3] (**VMEC** = **V**ariational **M**oments **E**quilibrium **C**ode) to calculate the MHD equilibrium state . This code generates free boundary equilibria with nested magnetic flux surfaces. The shape of the boundary between the plasma and the vacuum is determined by the pressure balance $B_p^2/2\mu_o + p = B_v^2/2\mu_o$ ($\mathbf{B}_p$ is the magnetic field inside the plasma boundary, p is the plasma pressure and $\mathbf{B}_v$ is the vacuum magnetic field) with vanishing normal component of the magnetic field at the boundary, $\mathbf{B}_v \cdot \hat{\mathbf{n}} = 0$.

The contravariant components of the VMEC magnetic field is given by

$$\mathbf{B}_e = \nabla\psi(s) \times \nabla\theta^* + \nabla v \times \nabla\chi_o(s), \tag{1}$$

where $2\pi\psi(s)$ and $2\pi\chi_o(s)$ are the toroidal and poloidal fluxes, respectively, s is a radial coordinate, v is the geometric toroidal angle and θ^* is a poloidal coordinate defined by

$$\theta^* = u + \lambda(s, u, v), \tag{2}$$

where u is the VMEC poloidal coordinate. We show the difference between these two poloidal coordinates in Fig. (1). Using the formalism of curvilinear

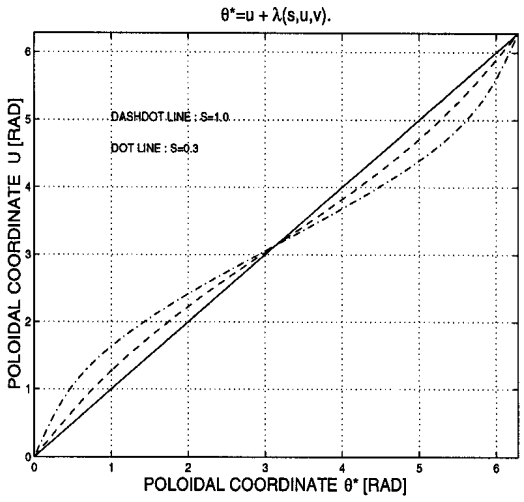

Figure 1: Definition of the poloidal coordinate $\theta^* = u + \lambda(s, u, v)$ for different values of s (solid line: $\theta^* = u$. Dashdot line: $s = 1.0$. Dot line: $s = 0.3$) .

coordinates and equation (2), equation (1) becomes

$$\mathbf{B}_e(s,u,v) = \underbrace{\frac{\psi'(s)}{\sqrt{g}}\left(\iota(s) - \frac{\partial\lambda}{\partial v}\right)}_{B_e^u}\mathbf{e}_u + \underbrace{\frac{\psi'(s)}{\sqrt{g}}\left(1 + \frac{\partial\lambda}{\partial u}\right)}_{B_e^v}\mathbf{e}_v, \tag{3}$$

where $\sqrt{g} = [\nabla s \times \nabla u \cdot \nabla v]^{-1}$ is the Jacobian of the transformation and ι the rotational transform.

The MFLT3D code obtains from the VMEC code the Fourier amplitudes of the contravariant components of the magnetic fields $(B^u_{mn}(s), B^v_{mn}(s))$, the poloidal angle renormalisation function lambda $(\lambda_{mn}(s))$, the Jacobian $(\sqrt{g}_{mn}(s))$, the cylindrical coordinates $(R_{mn}(s), Z_{mn}(s))$ that parameterize the flux surfaces, the toroidal and poloidal flux functions $\psi(s)$ and $\chi_o(s)$, respectively, and the rotational transform $(\iota(s))$. All interpolations required are performed with the NAG library function E01AAF [4].

2.2 Equations of magnetic field lines in VMEC coordinates

In the VMEC coordinates (s,u,v), the equations of the field lines are

$$\frac{ds}{dv} = \frac{\mathbf{B}\cdot\nabla s}{\mathbf{B}\cdot\nabla v} = \frac{B^s}{B^v}, \quad \frac{du}{dv} = \frac{\mathbf{B}\cdot\nabla u}{\mathbf{B}\cdot\nabla v} = \frac{B^u}{B^v} \tag{4}$$

where $\mathbf{B}$ is the sum of the equilibrium magnetic field $\mathbf{B}_e$ and a perturbation magnetic field $\delta\mathbf{B}$ whose contravariant components are given by

$$\delta B^s = \frac{R}{\sqrt{g}}\left[\delta B^Z\frac{\partial R}{\partial u} - \delta B^R\frac{\partial Z}{\partial u}\right]\Bigg|_{s,u,v} \tag{5a}$$

$$\delta B^u = \frac{R}{\sqrt{g}}\left[\delta B^R\frac{\partial Z}{\partial s} - \delta B^Z\frac{\partial R}{\partial s}\right]\Bigg|_{s,u,v} \tag{5b}$$

$$\delta B^v = \frac{\delta B^v}{R}\Big|_{s,u,v} \tag{5c}$$

where we have used the cylindrical components for $\delta\mathbf{B} = \delta B^R\hat{\mathbf{e}}_R + \delta B^v\hat{\mathbf{e}}_v + \delta B^Z\hat{\mathbf{e}}_Z$. Without the perturbation, the magnetic field lines form nested surfaces because $B^s \equiv 0$. With this choice of coordinates, an inverse transformation is not necessary as we have $R = R(s,u,v)$ and $Z = Z(s,u,v)$ directly.

2.3 Equations of the magnetic field lines in magnetic coordinates

If we analyze eq. (1) and if we take as new coordinates the triplet (ψ, θ^*, v), we can write for the contravariant components of the equilibrium field

$$\mathbf{B}_e \cdot \nabla\psi = -\frac{1}{\sqrt{g}_*}\frac{\partial \chi_o}{\partial \theta^*}, \tag{6a}$$

$$\mathbf{B}_e \cdot \nabla\theta^* = \frac{1}{\sqrt{g}_*}\frac{\partial \chi_o}{\partial \psi}, \tag{6b}$$

$$\mathbf{B}_e \cdot \nabla v = \frac{1}{\sqrt{g}_*}, \tag{6c}$$

where $\sqrt{g}_* = [\nabla\psi \times \nabla\theta^* \cdot \nabla v]^{-1}$. So we see that the equations of the magnetic field lines become

$$\frac{d\theta^*}{dv} = \frac{\mathbf{B}_e \cdot \nabla\theta^*}{\mathbf{B}_e \cdot \nabla v} = \frac{\partial \chi_o}{\partial \psi} \equiv \iota(\psi), \quad \frac{d\psi}{dv} = \frac{\mathbf{B}_e \cdot \nabla\psi}{\mathbf{B}_e \cdot \nabla v} = \frac{\partial \chi_o}{\partial \theta^*} \equiv 0.$$

We recognize here a Hamiltonian formulation (a non-autonomous system with one degree of freedom) where $H \leftrightarrow \chi_o$, $p \leftrightarrow \psi$, $q \leftrightarrow \theta^*$ and $t \leftrightarrow v$. Furthermore, we note that for a VMEC equilibrium $\chi_o = \chi_o(\psi)$ and thus our system is integrable (two constants of the motion χ_o, ψ exist) and the trajectories are straight in the phase space. In addition, we observe that the rotational transform plays the same role as the eigenfrequency in integrable conservative systems subjected to weak perturbations (KAM theory).

Unfortunately, this choice of coordinates does not allow our perturbation to be cast in a Hamiltonian form. On the other hand, following Refs. [5, 6, 7], we can express the perturbed Hamiltonian as

$$\delta\chi = -R\delta A^v, \tag{7}$$

hence the equations of the magnetic field lines become,

$$\frac{d\theta^*}{dv} = \iota(\psi) + \frac{\partial \delta\chi}{\partial \psi}, \quad \frac{d\psi}{dv} = -\frac{\partial \delta\chi}{\partial \theta^*} \tag{8}$$

where δA^v is the vector potential of the perturbation. In order to justify this form, we note that the vector potential $\delta\mathbf{A} = \delta A^R \hat{e}_R + \delta A^v \hat{e}_v + \delta A^Z \hat{e}_Z$, the magnetic field lines are given by,

$$\frac{d\theta^*}{dv} = \frac{\iota(\psi) + \frac{\partial \delta A_\psi}{\partial v} - \frac{\partial \delta A_v}{\partial \psi}}{1 + \frac{\partial \delta A_{\theta^*}}{\partial \psi} - \frac{\partial \delta A_\psi}{\partial \theta^*}}, \quad \frac{d\psi}{dv} = \frac{\frac{\partial \delta A_v}{\partial \theta^*} - \frac{\partial \delta A_{\theta^*}}{\partial v}}{1 + \frac{\partial \delta A_{\theta^*}}{\partial \psi} - \frac{\partial \delta A_\psi}{\partial \theta^*}}.$$

Therefore to put these equations into a Hamiltonian formalism, we have to make the following assumptions:

1. $\frac{\partial \delta A_{\theta^*}}{\partial \psi} - \frac{\partial \delta A_{\psi}}{\partial \theta^*} << 1 \leftrightarrow \delta \mathbf{B} \cdot \nabla v << \mathbf{B}_e \cdot \nabla v$ which is true in most cases.

2. $\frac{\partial \delta A_{\psi}}{\partial v} - \frac{\partial \delta A_v}{\partial \psi} \sim -\frac{\partial \delta A_v}{\partial \psi}$ and $\frac{\partial \delta A_v}{\partial \theta^*} - \frac{\partial \delta A_{\theta^*}}{\partial v} \sim \frac{\partial \delta A_v}{\partial \theta^*}$.

The last assumption implies $\frac{\partial \delta A^R}{\partial v} \sim 0$, $\frac{\partial \delta A^Z}{\partial v} \sim 0$ and $\frac{\partial R}{\partial v} \sim 0$, $\frac{\partial Z}{\partial v} \sim 0$ because $\delta A_{\psi} \equiv \delta A^R \frac{\partial R}{\partial \psi} + \delta A^Z \frac{\partial Z}{\partial \psi}$ and $\delta A_{\theta^*} \equiv \delta A^R \frac{\partial R}{\partial \theta^*} + \delta A^Z \frac{\partial Z}{\partial \theta^*}$, and this is not satisfied in general.

Consequently, we have to find another representation for the magnetic field lines in which the perturbation can be written in a Hamiltonian form without approximation.

2.4 Equations of magnetic field lines in canonical coordinates

We have seen that eq. (1) yields a Hamiltonian description for the magnetic field lines in the (ψ, θ^*, v) coordinates. We can write in general [8] that

$$\mathbf{B}(\mathbf{x}) = \nabla \Psi \times \nabla \theta^* + \nabla v \times \nabla \chi(\Psi, \theta^*, v). \tag{9}$$

and this representation satisfies automatically $\nabla \cdot \mathbf{B} = 0$. In this notation Ψ and χ are the toroidal and poloidal flux functions, respectively, and θ^* and v are the poloidal coordinate and geometric toroidal angle, respectively [9]. In these coordinates, the poloidal flux function depends on (Ψ, θ^*, v) contrary to the magnetic representation where it is a function of the toroidal flux function ψ only. This important difference allows complex trajectories in the phase space like stochastic solutions and magnetic islands. The magnetic field lines become

$$\frac{d\theta^*}{dv} = \frac{\partial \chi(\Psi, \theta^*, v)}{\partial \Psi}, \quad \frac{d\Psi}{dv} = -\frac{\partial \chi(\Psi, \theta^*, v)}{\partial \theta^*} \tag{10}$$

where we recognize the Hamiltonian formulation (a non-autonomous system with one degree of freedom) with $\chi \leftrightarrow H$, $\Psi \leftrightarrow p$, $\theta^* \leftrightarrow q$ and $v \leftrightarrow t$. To determine χ, we have to make the assumption that $\mathbf{B}$ can be written in the form

$$\mathbf{B}(\mathbf{x}) = \mathbf{B}_s(\mathbf{x}) + \delta \mathbf{B}(\mathbf{x})$$

where $\delta \mathbf{B}$ is a general magnetic field and $\mathbf{B}_s$ is a magnetic field with nested flux surfaces, hence the poloidal flux associated with this field is a function

of the toroidal flux only. Typically, this magnetic field corresponds to the VMEC magnetic field. This hypothesis implies the existence of magnetic coordinates (ψ, θ^*, v) for $\mathbf{B}_s$. Therefore, we can define a transformation of coordinates $\mathbf{x} = \mathbf{x}(\psi, \theta^*, v)$, with the Jacobian $\sqrt{g}_* = [\nabla\psi \times \nabla\theta^* \cdot \nabla v]^{-1}$, in which $\Psi = \Psi(\psi, \theta^*, v)$ and $\chi = \chi(\psi, \theta^*, v)$ [8, 9, 10]. Multiplying eq. (9) by $\sqrt{g}_* \nabla v$ and by $\sqrt{g}_* \nabla\theta^*$, we obtain

$$\frac{\partial \Psi}{\partial \psi}(\psi, \theta^*, v) = \sqrt{g}_* \mathbf{B} \cdot \nabla v\big|_{\psi,\theta^*,v}, \tag{11a}$$

$$\frac{\partial \chi}{\partial \psi}(\psi, \theta^*, v) = \sqrt{g}_* \mathbf{B} \cdot \nabla\theta^*\big|_{\psi,\theta^*,v}. \tag{11b}$$

and we can evaluate the Hamiltonian

$$\chi = \chi(\psi = \psi(\Psi, \theta^*, v), \theta^*, v) \tag{12}$$

where we have inverted the relation given by eq. (11a). Concerning the determination of χ, we have to resolve eqs. (11a) and (11b) on a 3-D mesh and then fit the solution. The choice of the initial condition is not important; we can take, for example, $\Psi(\psi = 0, \theta^*, v) = \psi_{vmec}(s = 0)$ and $\chi(\psi = 0, \theta^*, v) = \chi_{vmec}(s = 0)$.

Finally, we have to evaluate the contravariant components of the equilibrium magnetic field $\mathbf{B}_s \equiv \mathbf{B}_e$ and of the perturbed magnetic field $\delta\mathbf{B}$. Using eqs. (2) and (3), we obtain

$$\mathbf{B}_e \cdot \nabla v = B_e^v \tag{13a}$$

$$\mathbf{B}_e \cdot \nabla\theta^* = B_e^u(1 + \frac{\partial \lambda}{\partial u}) + B_e^v \frac{\partial \lambda}{\partial v} \tag{13b}$$

since

$$\nabla\theta^* = (1 + \frac{\partial \lambda}{\partial u})\nabla u + \frac{\partial \lambda}{\partial v}\nabla v + \frac{\partial \lambda}{\partial s}\nabla s.$$

Using the cylindrical coordinates for $\delta\mathbf{B}$ ($\delta\mathbf{B} = \delta B^R \hat{\mathbf{e}}_v \times \hat{\mathbf{e}}_Z + \delta B^v \hat{\mathbf{e}}_v + \delta B^Z \hat{\mathbf{e}}_R \times \hat{\mathbf{e}}_v$), we can write that

$$\delta\mathbf{B} \cdot \nabla v = \frac{\delta B^v}{R} \tag{14}$$

and

$$\delta \mathbf{B} \cdot \nabla \theta^* = \frac{R}{\sqrt{g}} \Bigg\{ \delta B^R \left[\left(1 + \frac{\partial \lambda}{\partial u} \right) \frac{\partial Z}{\partial s} - \frac{\partial \lambda}{\partial s} \frac{\partial Z}{\partial u} \right]$$

$$+ \delta B^Z \left[\frac{\partial \lambda}{\partial s} \frac{\partial R}{\partial u} - \left(1 + \frac{\partial \lambda}{\partial u} \right) \frac{\partial R}{\partial s} \right] \Bigg\} + \frac{\delta B^v}{R} \frac{\partial \lambda}{\partial v} \tag{15}$$

where $\sqrt{g} = [\nabla s \times \nabla u \cdot \nabla v]^{-1}$. With regards to the expression for $\sqrt{g}_* = [\nabla \psi \times \nabla \theta^* \cdot \nabla v]^{-1}$, we use the relation for $\nabla \theta^*$ and $\nabla \psi = \psi'(s) \nabla s$ to obtain

$$\sqrt{g}_* = \frac{1}{\psi'(s)\left(1 + \frac{\partial \lambda}{\partial u}\right) \nabla s \times \nabla u \cdot \nabla v} = \frac{\sqrt{g}}{\psi'(s)\left(1 + \frac{\partial \lambda}{\partial u}\right)} \equiv \frac{1}{B_e^v} \tag{16}$$

We recall that in eqs. (14-16), we invert the relation ($s = s(\psi)$, $u = u(\psi, \theta^*, v)$, v). In this way, it is not necessary to broaden the VMEC spectrum. To map from (ψ, θ^*, v) to (s, u, v), we use the system

$$\psi(s) - \bar{\psi} = 0,$$

$$u + \lambda(s, u, v) - \bar{\theta}^* = 0.$$

where $\bar{\psi}$ and $\bar{\theta}^*$ are known. The solution is obtained with the NAG library routine C05NBF [11, 12]. The transformation from (Ψ, θ^*, v) to (ψ, θ^*, v) requires the application of eq. (11a):

$$\Psi(\psi, \theta^*, v) - \bar{\Psi} = 0.$$

Therefore we can map from $(\Psi, \theta^*, v) \rightarrow (\psi, \theta^*, v) \rightarrow (s, u, v)$.

3 Numerical results

The JET Tokamak has an iron core with 8 legs in which a magnetic flux flows to induce an ohmic current in the plasma. The flux can saturate and leak from the structure. We can model this flux with a vertical magnetic field modulated toroidally. As a model, we use a system of vertical field coil filaments formed by two symmetric (with respect to the plane $z = 0$) octahedrons with current δI_p superimposed on two circular loops with current $-\delta I_p$ (Fig. 2).

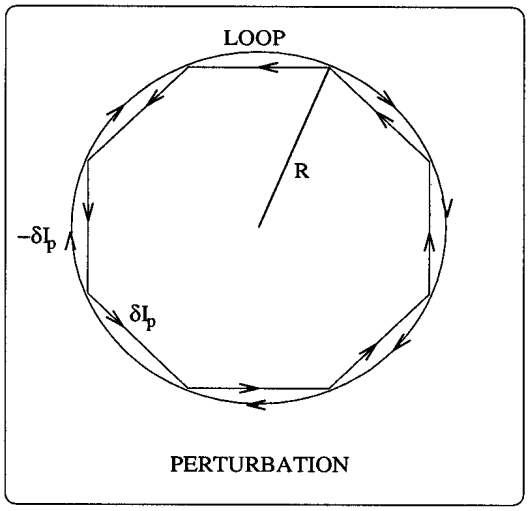

Figure 2: System of vertical field coil filaments formed by two symmetric octahedrons with current δI_p superimposed on two circular loops with current $-\delta I_p$ which model the effect of the flux leakage from the saturated iron core.

To compute the magnetic field we use the Biot-Savart Law and the evaluation of the vector potential is carried out with the formula

$$\mathbf{A}(\mathbf{x}) = \frac{\mu_o}{4\pi} \int_{wire} \frac{I d\mathbf{l}}{|\mathbf{x} - \mathbf{x}'|}.$$

The calculations to determine the magnetic field line trajectories inside the plasma boundary are undertaken with the application of eqs. (4), (8) and (10). The Chirikov parameter and the Liapunov exponent are also evaluated. The dimensions of the model vertical coil filaments are $R = 3.2\ m, h = \pm 2.5m$ with current $\delta I_p = 0.1 MA$. With this choice of parameters the ratio between δB^s and B_e^v is approximatively 0.1%.

For the VMEC equilibrium, we have used a linear profile for the current and for the pressure in order to obtain a $\beta \sim 3.21\%$ and a plasma current

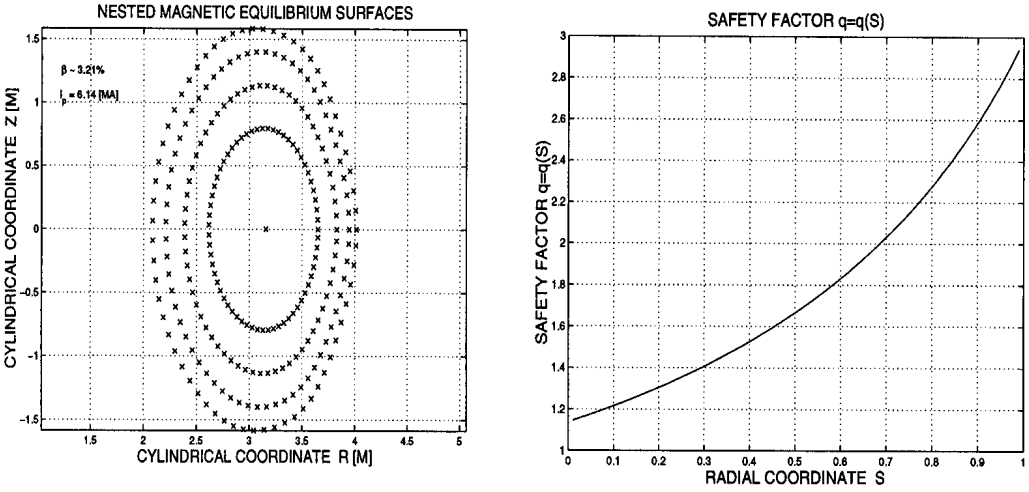

Figure 3: a) Different flux surfaces of the VMEC equilibrium (left). b) Safety factor profile q of the VMEC equilibrium as a function of s (right).

$I_p \sim 6.14\, MA$. This value of β is actually higher than has been presently obtained in JET high current discharges. The profile of the safety factor and a set of flux surfaces are displayed in Fig. 3. Because of the modulation of the toroidal magnetic field, we have to treat the JET as a 3-D configuration. In fact, if we impose an axisymmetric case, the VMEC code does not converge. For this reason, the spectrum of the equilibrium computation with VMEC include $0 \leq m \leq 7$ and $-3 \leq n/L \leq 3$, where m is the poloidal mode number, n is the toroidal mode number (per period) and $L = 32$ is the number of the toroidal coils. To compare the three different methods to determine magnetic field lines, we examine the right hand sides of the relevant equations (4), (8) and (10).

Fig. 4a (application of Sec. 2.2) shows the behavior of B^s/B^v for different values of s. Because of $B^s \neq 0$, the perturbation displaces the field line from the unperturbed flux surfaces. To understand this figure, we can compare it with Fig. 4b (circles). When $B^s/B^v \geq 0$ ($B^s/B^v \leq 0$) the magnetic field lines are pushed radially outwards (radially inwards). Consequently, when $0 \leq u \leq 1$ ($1 \leq u \leq 2$) and $4 \leq u \leq 5.5$ ($5.5 \leq u \leq 6.0$), we have that $ds/du > 0$ ($ds/du < 0$) which is confirmed in Fig. 4b (circles). Moreover when $d(B^s/B^v)/du = 0$, we have saddle points for the trajectories ($u \sim 0.8, 1.5, 4.6, 5.5$). From all this, it follows that B^s/B^v measures the transition rate across unperturbed flux surfaces. Fig. 4c constitutes a measure of the rotational transform. However, this cannot be fully appreciated

in the (s, u, v) coordinates. Canonical coordinates provide a more insightful picture. Fig. 5a (application of Sec. 2.3) and 5b (application of Sec. 2.4) have similar meaning to Fig. 4a. Therefore, the comments we have made about the implications of the variations of B^s/B^v are applicable to $-\partial\chi/\partial\theta^*$ and $-\partial\delta\chi/\partial\theta^*$ too. Comparing Figs. 4a, 5a and 5b, we note that the behavior of the curve B^s/B^v is closer to $-\partial\chi/\partial\theta^*$ in Fig. 5b than $-\partial\delta\chi/\partial\theta^*$ in Fig. 5a.

Concerning the profile of the rotational transform, Figs. 6a and 6b demonstrate the weak influence of the perturbation on it. The weak modulations in Fig. 6b are attributed to the discretisation of ψ during the resolution of eq. (11a).

The behavior of the trajectories in the phase space (s, u) are displayed in Fig. 4b. In this space, we have to solve eq. (4), (8) and (10) and to invert $(\Psi, \theta^*) \rightarrow (\psi, \theta^*) \rightarrow (s, u)$ and $(\psi, \theta^*) \rightarrow (s, u)$. We observe that the trajectory calculated with eq. (10) (Sec. 2.4) resembles the trajectory computed with the help of the eq. (4) (Sec. 2.2) except for some values around $u \sim 3$. The reason is that when we resolve the eqs. (11a) and (11b), we have not used the initial conditions $\psi = \psi_{vmec}(s = 0)$, because the VMEC values near the magnetic axis are not fully reliable. Thus, we have taken as the initial conditions

$$\chi(\psi = 0.05, \theta^*, v) = \chi_{nemec}(\psi = 0.05),\ \Psi(\psi = 0.05, \theta^*, v) = 0.05\,.$$

This can account for the difference between the two trajectories. If we look at the trajectory calculated with eq. (8) (Sec. 2.3), we observe that it differs significantly compared with the trajectory computed with eq. (4) (Sec. 2.2). But if we estimate the error between the three trajectories, we can determine the physical distance in the cylindrical coordinates at any given value of u calculated with the analytic and numerical Hamiltonian methods compared with that obtained from the nonHamiltonian approach. The maximal error with the numerical Hamiltonian is $\sim 0.5\,mm$, but it exceeds $3\,mm$ with the analytic Hamiltonian as shown in Fig. 7. This difference results from the assumptions made to obtain the analytic Hamiltonian (Sec. 2.3), particulary the fact that $\frac{\partial\delta A^R}{\partial v}$ is not equal to zero.

Finally, we observe that the flux leakage can cause island formation on a surface with rational values of the rotational transform. When $\iota = 8/22$ ($\iota = 8/23$), then there are 22 (23) island structures that are generated (Figs. 8, 9). Stochastic solutions are not induced because the Chirikov parameter is $\sim 1.02 \times 10^{-2}$ and which is smaller than unity. Thus, there is not an overlap between the two resonances 8/22 and 8/23. To evaluate this parameter we

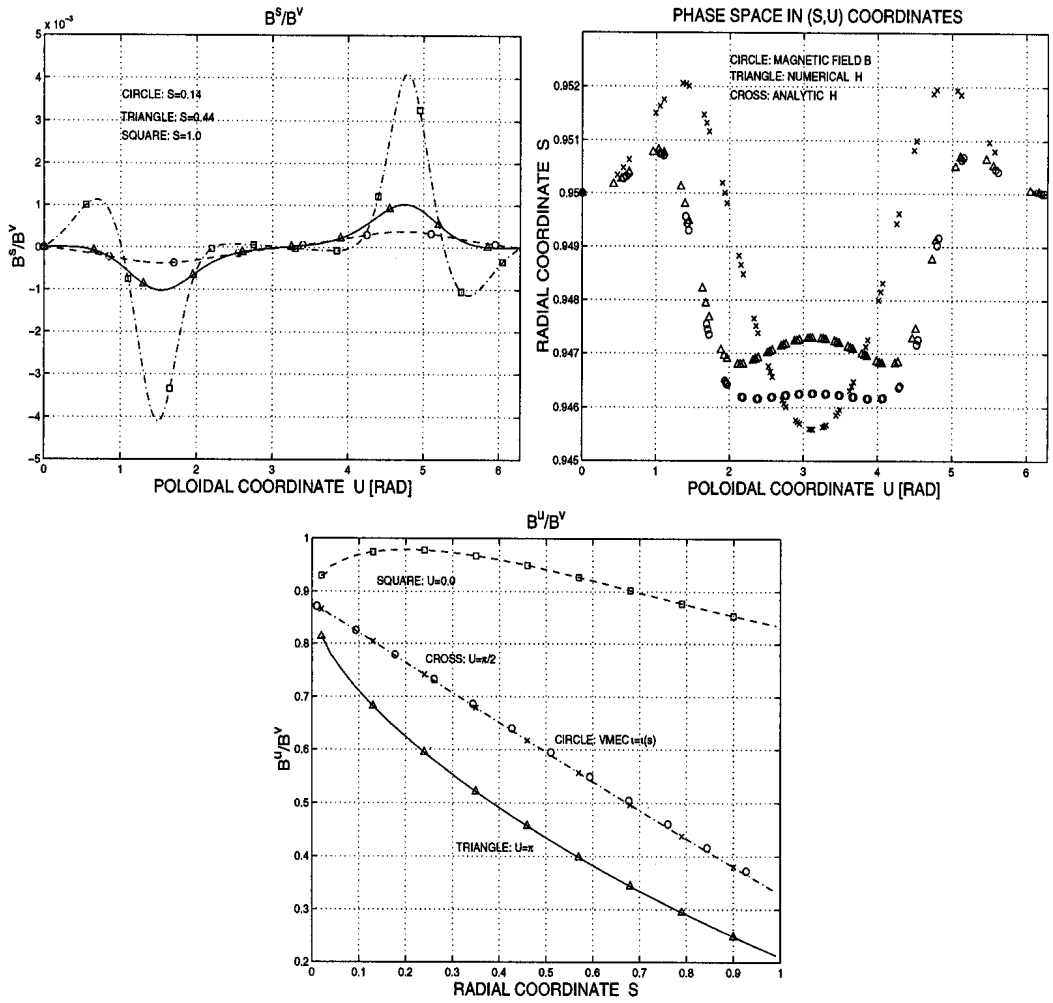

Figure 4: a) B^s/B^v as a function of u for different values of s (top left) (Circles: $s = 0.14$. Triangles: $s = 0.44$. Squares: $s = 1.0$). b) Trajectories of the magnetic field lines in (s, u) coordinates (top right) (Circles: in using the magnetic fields (eq. (4)). Crosses: in using the analytic Hamiltonian $\delta\chi$ (eq. (8)). Triangles: in using the numerical Hamiltonian χ (eq. (10))). c) B^u/B^v as a function of s for different values of u (bottom) (Squares: $u = 0.0$. Crosses: $u = \pi/2$. Triangles: $u = \pi$. Circles: ι of the VMEC equilibrium).

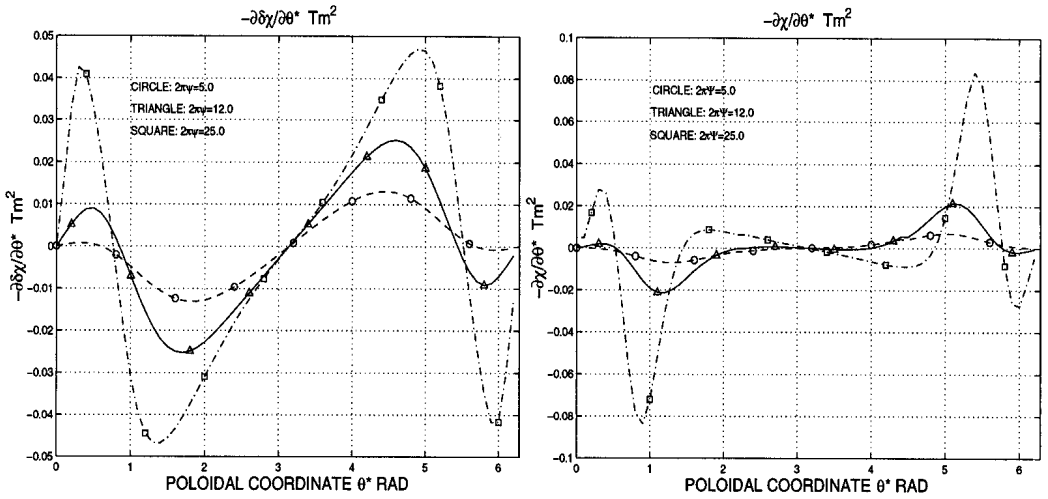

Figure 5: a) $-\partial\delta\chi/\partial\theta^*$ of the analytic Hamiltonian as a function of θ^* for different values of ψ (left) (Circles: $2\pi\psi = 5.0$. Triangles: $2\pi\psi = 12.0$. Squares: $2\pi\psi = 25$). b) $-\partial\chi/\partial\theta^*$ of the numerical Hamiltonian as a function of θ^* for different values of Ψ (right) (Circles: $2\pi\Psi = 5.0$. Triangles: $2\pi\Psi = 12.0$. Squares: $2\pi\Psi = 25$).

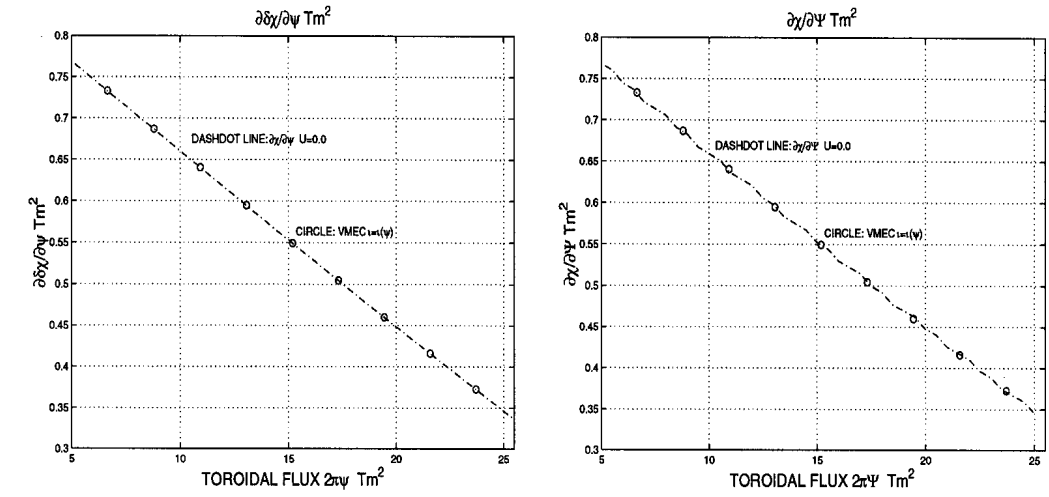

Figure 6: a) $\partial\delta\chi/\partial\psi$ of the analytic Hamiltonian as a function of ψ (left) and b) $\partial\chi/\partial\Psi$ of the numerical Hamiltonian as a function of Ψ (right) (Dasdot line: $u = 0.0$. Circle: ι of the VMEC equilibrium) .

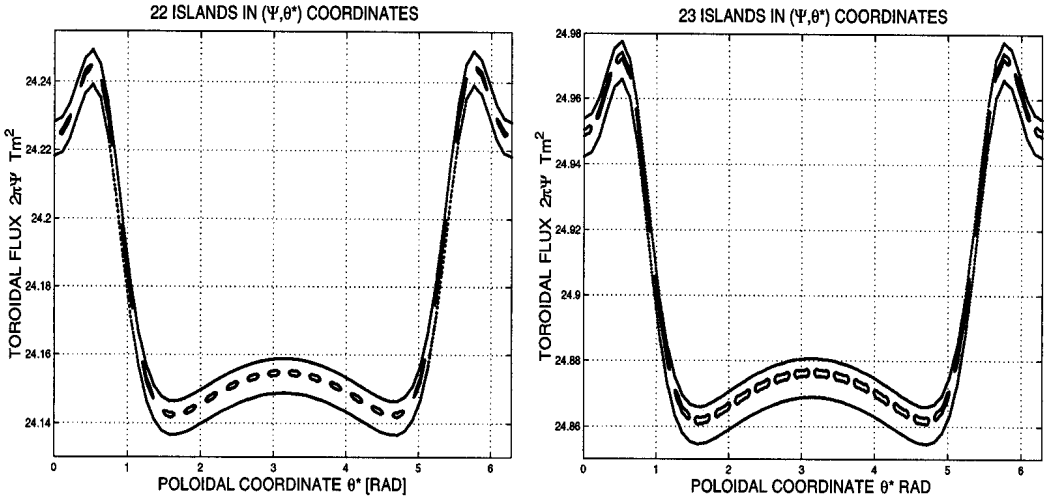

Figure 9: a) The 22 magnetic island structures (left) and b) 23 (right) computed with the numerical Hamiltonian χ (eq. (10)).

have used the formula [5, 7, 13, 14, 17]:

$$\sigma(\hat{\Psi}_{mn}, \hat{\Psi}_{m+1,n}) \sim 2\frac{\sqrt{\left|\frac{\delta\chi_{mn}}{\frac{d\iota}{d\Psi}}|_{\hat{\Psi}_{mn}}\right|} + \sqrt{\left|\frac{\delta\chi_{m+1,n}}{\frac{d\iota}{d\Psi}}|_{\hat{\Psi}_{m+1,n}}\right|}}{\frac{1}{n}\left|\frac{1}{\frac{dq}{d\Psi}|_{\hat{\Psi}_{mn}}}\right|}.$$

To conclude, if we estimate the biggest Liapunov exponent [15, 16, 17], we note that it tends towards zero ($\lambda(N) \sim cteN^{-0.644}$) (Fig. 10) and we conclude that the perturbation does not produce a stochastic solution. Initially adjacent field lines do not separate.

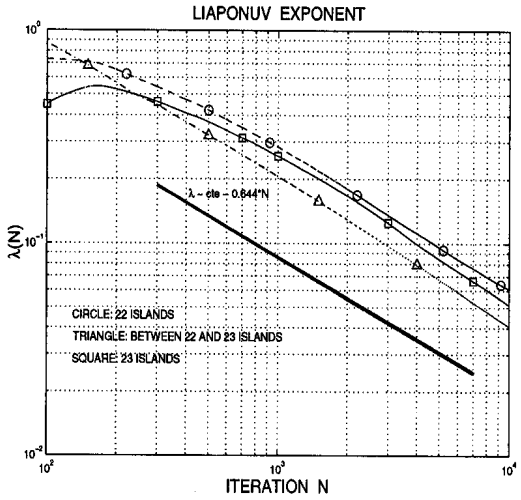

Figure 10: Liapunov exponent for different initial conditions (Circles: in the 22 magnetic island structures. Triangles: in the 23 magnetic island structures. Squares: between 22 and 23 magnetic island structures. Solid line: comportment of the Liapunov exponent $\lambda(N) \sim cteN^{-0.644}$).

4 Conclusion

We have shown that a Hamiltonian representation of the magnetic field lines in a 3-D free boundary equilibrium subject to a magnetic perturbation is possible. The Hamiltonian formulation allows the application of the formalism developed for Hamiltonian systems [17]. The comparison of the trajectories between the three different methods described in Secs. 2.2, 2.3 and 2.4 yield similar results. Although the approximate analytic Hamiltonian approach we have investigated can displace the orbits locally up to 0.5 cm from the correct position (Fig. 7).

The method we have applied superimposes a perturbation of a 3-D equilibrium with perfectly nested magnetic surfaces. A more self consistent approach would require the application of a more general 3-D MHD equilibrium code that can treat magnetic islands and stochastic regions like the PIES code [18], but modified to account for the variable permeability μ in the iron core. For small perturbations around an equilibrium state, these types of codes may be extremely time consuming and expensive to operate.

We have investigated the effect of the magnetic flux leakage from the saturated iron core of a model of the JET tokamak and have detected the formation of island structures on surfaces with rational values of the rotational transform $\iota = 8/22$ and $\iota = 8/23$. However, we have not observed a stochastic solution for the magnetic field lines inside the plasma boundary. To verify this, we have computed parameters such the Chirikov parameter and the Liapunov exponent. The calculation of the Chirikov parameter demonstrates that it is smaller than unity and thus there is no overlap between the two resonances (there is not an overlap between the two islands structures and so the solution is stable). The Liapunov exponent yields an estimate of the divergence of initially adjacent field lines and we have observed that it tends towards zero.

We have also looked at a different model for the flux leakage of the iron core. Eight up-down symmetric frames formed by pairs of adjacent filaments in which current flows radially inwards in one filament and radially outward in its neighbor set up the toroidally modulated vertical field. Island formation without a stochastic solution was also observed. Applying the three different methods of resolution, we have obtained very similar results as those with the model described in this paper.

Finally, it will be necessary to calculate more precisely the VMEC values near the magnetic axis in order to optimize the calculation of the Hamiltonian. We could use the Hamiltonian version of the MFLT3D code to make investigations on the magnetic topology of a perturbation in a 3-D free